Selective Oxidation of Methanol and Ethanol on Supported Ruthenium Oxide Clusters at Low Temperatures†

Haichao Liu and Enrique Iglesia*

Department of Chemical Engineering, University of California at Berkeley, and Chemical Sciences Division, E.O. Lawrence Berkeley National Laboratory, Berkeley, California 94720

Received: March 4, 2004

RuO_2 domains supported on SnO_2, ZrO_2, TiO_2, Al_2O_3, and SiO_2 catalyze the oxidative conversion of methanol to formaldehyde, methylformate, and dimethoxymethane with unprecedented rates and high combined selectivity (>99%) and yield at low temperatures (300−400 K). Supports influence turnover rates and the ability of RuO_2 domains to undergo redox cycles required for oxidation turnovers. Oxidative dehydrogenation turnover rates and rates of stoichiometric reduction of RuO_2 in H_2 increased in parallel when RuO_2 domains were dispersed on more reducible supports. These support effects, the kinetic effects of CH_3OH and O_2 on reaction rates, and the observed kinetic isotope effects with CH_3OD and CD_3OD reactants are consistent with a sequence of elementary steps involving kinetically relevant H-abstraction from adsorbed methoxide species using lattice oxygen atoms and with methoxide formation in quasi-equilibrated CH_3OH dissociation on nearly stoichiometric RuO_2 surfaces. Anaerobic transient experiments confirmed that CH_3OH oxidation to HCHO requires lattice oxygen atoms and that selectivities are not influenced by the presence of O_2. Residence time effects on selectivity indicate that secondary HCHO−CH_3OH acetalization reactions lead to hemiacetal or methoxymethanol intermediates that convert to dimethoxymethane in reactions with CH_3OH on support acid sites or dehydrogenate to form methylformate on RuO_2 and support redox sites. These conclusions are consistent with the tendency of Al_2O_3 and SiO_2 supports to favor dimethoxymethane formation, while SnO_2, ZrO_2, and TiO_2 preferentially form methylformate. These support effects on secondary reactions were confirmed by measured CH_3OH oxidation rates and selectivities on physical mixtures of supported RuO_2 catalysts and pure supports. Ethanol also reacts on supported RuO_2 domains to form predominately acetaldehyde and diethoxyethane at 300−400 K. The bifunctional nature of these reaction pathways and the remarkable ability of RuO_2-based catalysts to oxidize CH_3OH to HCHO at unprecedented low temperatures introduce significant opportunities for new routes to complex oxygenates, including some containing C−C bonds, using methanol or ethanol as intermediates derived from natural gas or biomass.

1. Introduction

Methanol oxidation reactions lead to formaldehyde (HCHO), dimethoxymethane ($CH_3OCH_2OCH_3$, DMM), and methylformate ($HCOOCH_3$, MF) products. Oxidative routes to HCHO are practiced on silver-based and iron-molybdate catalysts.[1] Methylformate, a precursor to formamides, carboxylic acids, and their ethers,[1,2] is produced via (nonoxidative) CH_3OH dehydrogenation on CuO or carbonylation using liquid bases.[2,3] The direct oxidative conversion of methanol to methylformate occurs only at modest reaction rates.[2−5] DMM is produced in a two-step process involving methanol oxidation to HCHO followed by acetalization of HCHO−CH_3OH mixtures with liquid or solid acids. Direct CH_3OH oxidation with significant DMM yields has been recently reported on ReO_x-based catalysts[6] and on polyoxometalate Keggin clusters.[7]

CH_3OH oxidation to MF on MoO_x and VO_x catalysts involves rate-determining C−H activation steps to form HCHO and subsequent HCHO reactions with intermediates derived from CH_3OH or HCHO.[1,8,9] These intermediates also form CO_x at conditions required for HCHO synthesis. Acid-catalyzed acetalization is favored by thermodynamics at low temperatures;[10] current DMM synthesis routes form dimethyl ether and CO_x as undesired byproducts. Higher MF and DMM selectivities will require that HCHO intermediates be formed at lower temperatures than on existing catalysts.

RuO_2 domains catalyze CO oxidation (at ambient temperatures),[11] as well as the oxidation of C_{5+} alcohols to aldehydes and ketones (at ∼373 K).[12−14] Here, we report unprecedented methanol and ethanol oxidation rates and selectivities on RuO_2 domains at very low temperatures (300−400 K) and a specific role of supports in directing HCHO−CH_3OH reactions toward MF or DMM products with high selectivity. We probe the redox character of the catalytic sequence, the nature of the kinetically relevant steps, and the relation between reduction dynamics and catalytic reactivity of RuO_2 domains. These findings suggest selective routes to a broad range of complex oxygen-containing products via oxidative reactions of methanol and ethanol.

2. Experimental Section

Supported RuO_2 catalysts were prepared by incipient wetness impregnation of $ZrO_{2-x}(OH)_{2x}$, $Sn(OH)_4$, TiO_2 (Degussa, P25), Al_2O_3 (Alcoa, HiQ31), SiO_2 (Cab-O-Sil), and MgO with aqueous solutions of $Ru(NO)(NO_3)_3 \cdot xH_2O$ (Aldrich, 56 wt % Ru) at 298 K for 5 h. Impregnated supports were dried in ambient air at 398 K overnight and then in flowing dry air

† Part of the special issue "Michel Boudart Festschrift".

* To whom correspondence should be addressed. E-mail: iglesia@cchem.berkeley.edu; tel.: (510) 642-9673; Fax: (510) 642-4778.

10.1021/jp0401980 CCC: $27.50
Published on Web 00/00/0000 PAGE EST: 8.1

(Airgas, zero grade, 0.7 cm^3/g-s) at 673 K for 2 h. $ZrO_{2-x}(OH)_{2x}$, $Sn(OH)_4$, and MgO were prepared as in previous reports.[15] $ZrO_{2-x}(OH)_{2x}$ was prepared by hydrolysis of aqueous zirconyl chloride solutions (>98%, Aldrich) at a pH of ~10 using NH_4OH (14.8 N, Fisher Scientific), followed by filtration of precipitated powders, and treatment in ambient air at 393 K overnight. SnO_2 was prepared by hydrolysis of tin (IV) chloride pentahydrate (98%, Alfa Aesar) at a pH of ~7 using NH_4OH (14.8 N, Fisher Scientific), followed by treatment of the resulting solids in dry air (Airgas, zero grade, 0.7 cm^3/g-s) at 773 K for 3 h. MgO was prepared by contacting MgO (>98%, Aldrich) with deionized water at 355−365 K for 4 h, and then treating samples in flowing dry air (Airgas, zero grade, 0.7 cm^3/g-s) at 773 K for 8 h. Al_2O_3 was treated in flowing dry air at 823 K for 5 h before use.

The nominal Ru surface density for each sample is reported as Ru/nm^2, based on the Ru content and BET surface area for each sample. Surface areas were measured using N_2 at its normal boiling point (Autosorb-1; Quantachrome) and BET analysis methods. The dispersion of Ru crystallites was measured using H_2 chemisorption at 313 K after reduction of RuO_2 domains in H_2 at 573 K for 1 h (Autosorb-1; Quantachrome). Repeated reduction−oxidation cycles did not influence measured dispersions, indicating that the resulting metal crystallites represent a reasonable relative measure of the dispersion of RuO_2 clusters present during oxidation catalysis.

Reduction rates of supported RuO_2 domains in H_2 were measured using a Quantachrome analyzer (Quantachrome Corp.) modified with electronic flow controllers. Samples (2 mg Ru) were placed in a quartz cell (4 mm I.D.) containing a quartz well in contact with samples and heated linearly from 298 to 793 K at 0.167 K s^{-1} in flowing 20% H_2/Ar (1.33 cm^3 s^{-1}) (Matheson UHP). The H_2 content in the effluent was measured by thermal conductivity after H_2O formed during reduction was removed from the effluent using a 13X sieve trap at ambient temperature. The thermal conductivity detector was calibrated by reducing CuO powder in H_2 (99.995%, Aldrich). Reduction rates were measured from H_2 consumption rates using previously reported protocols.[15,16]

Methanol reactions were carried out in a packed-bed quartz microreactor. Catalyst powders (0.1−0.3 g) were diluted with quartz powder (~0.5 g) to prevent temperature gradients and treated in 20% O_2/He (O_2, Praxair, 99.999%; He, Airgas, 99.999%; 0.67 cm^3/s) flow at 573 K for 1 h before catalytic measurements. Reactants were 4 kPa CH_3OH (Merck, 99.99%), 9 kPa O_2, 1 kPa N_2 (Praxair, Certified O_2/N_2 mixture) and 86 kPa balance He (Airgas, 99.999%). The kinetic effects of CH_3OH (4−40 kPa) and O_2 (4.5−28 kPa) pressures on CH_3OH reaction rates and selectivities were also examined. Similar procedures were used for CH_3OH and C_2H_5OH (99.5% Aldrich) reactants. CH_3OD (CDN Isotopes, 99.6 at. % D) and CD_3OD (Cambridge Isotopes, 99.8 at. % D) were used as reactants to measure kinetic isotope effects.

Reactants and products were analyzed by on-line gas chromatography (Hewlett-Packard 6890GC) using a methyl-silicone capillary column (HP-1; 50 m × 0.25 mm, 0.25 μm film thickness) and a Porapak Q packed column (80−100 mesh, 1.82 m × 3.18 mm) connected to flame ionization and thermal conductivity detectors, respectively. Selectivities are reported on a carbon basis as the percentage of the converted CH_3OH appearing as a given product. Rates are reported as the molar CH_3OH conversion rates per total Ru or surface Ru atom. Blank experiments using empty reactors did not lead to detectable CH_3OH conversions at any of the conditions of our study.

Anaerobic CH_3OH reactions were carried out in transient mode using a packed-bed quartz microreactor to determine the role of lattice oxygen atoms and the involvement of redox pathways in CH_3OH oxidation on RuO_2 domains. Samples (0.1−0.3 g) were diluted with quartz powder (~0.5 g) and treated in 20% O_2/He (O_2, Praxair, 99.999%; He, Airgas, 99.999%; 0.67 cm^3/s) flow at 573 K for 1 h. Steady-state CH_3OH oxidation reactions were carried out in 4 kPa CH_3OH (1 cm^3(STP) s^{-1} Merck, 99.99%), 9 kPa O_2, 1 kPa N_2 (Praxair, Certified O_2/N_2 mixture) with He as balance (Airgas, 99.999%) before this reactant mixture was flushed with pure He (1 cm^3 s^{-1}) for 300 s. Then, a mixture CH_3OH (4 kPa) diluted with He was passed over the samples until CH_3OH conversion was no longer detected. Finally, O_2 was introduced into this CH_3OH/He mixture to confirm the recovery of initial catalytic oxidation turnover rates after these anaerobic transients. Reactants and products were analyzed every 8 s using on-line mass spectroscopy (Hewlett-Packard 5972, mass selective detector) during these experiments.

3. Results and Discussion

Table 1 shows CH_3OH oxidation rates (normalized by either total or surface-exposed Ru atoms) and selectivities at 393 K on RuO_2 domains supported on SiO_2, Al_2O_3, ZrO_2, TiO_2, SnO_2, and MgO with similar Ru fractional dispersion (0.174−0.215) and crystallite diameters (6.0−7.6 nm; from Ru dispersion assuming hemispherical crystallites). Raman spectra for these samples showed that RuO_2 species were well-dispersed on support surfaces, as evidenced by weak Raman features at 533, 637, and 712 cm^{-1} (data not shown), corresponding to E_g, A_{1g}, and B_{2g} modes, respectively.[17] The weak nature of these features is consistent with small RuO_2 structures, as also inferred from measured chemisorption uptakes on reduced forms of these samples.

HCHO, MF, DMM, and CO_2 were detected as products; neither CO nor dimethyl ether products were detected. Rates and selectivities are compared at similar CH_3OH conversions (~20%) in Table 1, because relative contributions of primary and secondary reactions depend on residence time and CH_3OH conversion, as discussed later. CH_3OH turnover rates were higher on RuO_2 supported on SnO_2, ZrO_2, and TiO_2 than on Al_2O_3 or SiO_2, while RuO_2 supported on MgO led to nearly undetectable CH_3OH conversions. Turnover rates changed by less than 5% during catalytic experiments (~15 h). Bulk RuO_2 (Aldrich, 99.9%) with relatively low surface area gave very low CH_3OH conversion rates (Table 1). Pure supports did not give detectable CH_3OH conversion rates in the absence of RuO_2, even at 473 K, a temperature much higher than required for significant conversions on RuO_2-containing samples.

As discussed below, CH_3OH oxidation requires rate-determining C−H activation in CH_3OH-derived methoxide intermediates to form HCHO through redox cycles using lattice oxygen atoms within RuO_x domains. HCHO then reacts in subsequent reactions with CH_3OH to form hemiacetal or methoxymethanol intermediates (CH_3OCH_2OH),[5] which can undergo condensation reactions with CH_3OH to form DMM or sequential hydrogen abstraction to form MF (Scheme 1). Reactions listed along the horizontal direction in Scheme 1 require acid sites, while those depicted along the vertical direction involve some reactive form of lattice oxygen (O*) on either RuO_2 domains or active supports.

The irreversible nature of the oxidative conversion of CH_3OH to HCHO requires one oxidative CH_3OH dehydrogenation (ODH) event for each HCHO, DMM, and MF molecule formed.

TABLE 1: Methanol Oxidation Rates and Selectivities on Supported RuO_2 Catalysts at Similar Methanol Conversion (~20%),[a] and on Previously Reported Catalysts

catalyst (Ru wt %)	Ru surface density (Ru/nm^2)	temperature/ CH_3OH pressure (K/kPa)	CH_3OH conversion rate (mol/g-atom M_{total}-h)	turnover rate (mol/g-atom Ru_{surf}-h)	calculated ODH turnover rate[b] (mol/g-atom Ru_{surf}-h)	initial reduction rate (mol H_2/ g-atom Ru-h)	selectivity (%) HCHO	MF	DMM	CO_x
RuO_2/SiO_2 (4.3%)	1.1	393/4	8.3	41.5	19.4	5.3	12.4	31.0	56.1	0.6
RuO_2/Al_2O_3 (4.4%)	1.3	393/4	14.9	71.0	32.5	7.5	11.6	30.1	57.4	1.0
RuO_2/ZrO_2 (4.1%)	2.1	393/4	17.6	88.9	53.2	11.6	6.6	70.7	5.6	16.8
RuO_2/TiO_2 (2.2%)	3.1	393/4	14.5	84.7	52.1	10.8	25.2	69.9	4.1	0.9
RuO_2/SnO_2 (4.1%)	2.5	393/4	30.6	142.3	79.1	22.3	20.0	60.7	15.5	3.8
RuO_2/SnO_2 (4.1%)	2.5	333/4	2.0	9.3	5.0		10.2	83.1	6.7	0
RuO_2/SnO_2[c] (4.1%)	2.5	333/80	4.3	19.9	8.7		1.6	57.3	40.8	0
RuO_x/Al_2O_3[c] (4.4%)	1.3	333/80	2.0	9.5	4.1		9.4	23.4	66.8	0.4
RuO_2/MgO (4.3%)	2.3	393/4	0.3	1.7	1.4	0.4				
bulk RuO_2		393/4	2.3	26.7[h]	16.6[h]		34.9	53.5	2.2	9.4
$V_2O_5-TiO_2$[(2)d]		443/9	3.4				7	80	3	5
$Mo-Sn-O$[(3)e]		433/6	1.0				5	90	0	2
$Mo-Sn-O$[(4)f]		453/18	1.8				27.2	47.0	0	1.5
MoO_3/SiO_2[(5)g]		533/7	1.1					95.9	-	3.0

[a] Ru dispersion: 0.174−0.215, 9 kPa O_2, 1 kPa N_2. [b] Rate for primary CH_3OH oxidative dehydrogenation to HCHO. [c] 80 kPa CH_3OH, 18 kPa O_2, 2 kPa N_2. [d] ~9 kPa CH_3OH, ~10 kPa O_2, balance N_2, V/Ti (atomic ratio) = 0.0375. [e] ~6 kPa CH_3OH, ~4 kPa O_2, balance N_2, Mo/Sn (atomic ratio) = 3/7. [f] 18 kPa CH_3OH, 7 kPa O_2, balance He, Mo/Sn (atomic ratio) = 3/7. [g] 7 kPa CH_3OH, 19 kPa O_2, balance He, 0.18 wt % Mo. [h] Estimated by assuming the number of surface Ru atoms to be $10^{19}/m^2$ for the bulk RuO_2.

SCHEME 1: Proposed Primary and Secondary CH_3OH Reaction Pathways

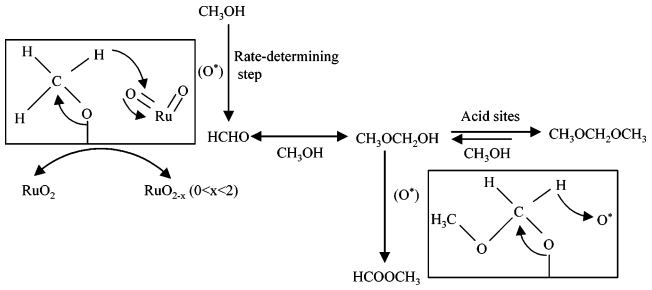

Thus, ODH rates are reported as the combined molar formation rates of these products; ODH rates rigorously reflect the intrinsic oxidation reactivity of active domains, without contributions from methanol molecules consumed because of various secondary reactions. ODH turnover rates (per exposed Ru) are ~1.5 times greater when RuO_2 was supported on SnO_2 than on ZrO_2 and TiO_2 and 2.5−4 times greater than when supported on Al_2O_3 and SiO_2 (Table 1). ODH rates are much lower and near our detection limits (~0.1 mol/g-atom-Ru-h) on RuO_2/MgO.

SnO_2 supports led to RuO_x domains with the highest reactivity, to significant reaction rates even near ambient temperatures (333 K), and to combined selectivities to MF, HCHO, and DMM above 99% (and 83% MF selectivity) at 10% CH_3OH conversion (Table 1). Higher CH_3OH pressures (80 vs 4 kPa) increased reaction rates (by a factor of 2) and DMM selectivities (6.7 to 40.8%) at the expense of lower MF selectivities (83.1 to 57.3%). These CH_3OH pressure effects are similar to those observed on RuO_2/Al_2O_3 (Table 1); they reflect secondary DMM synthesis pathways influenced by thermodynamic constraints that become less severe as CH_3OH pressure increases.

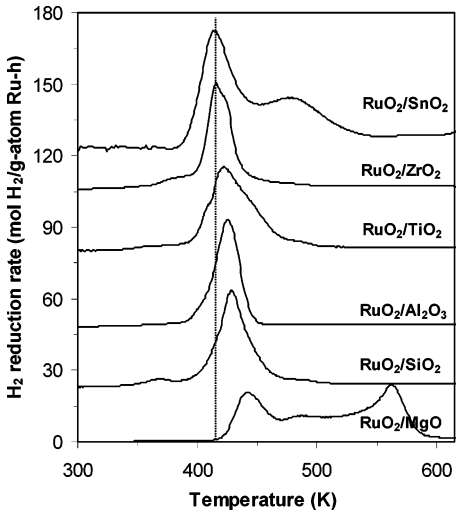

Figure 1. Temperature-programmed reduction profiles for RuO_2 domains supported on SnO_2, ZrO_2, TiO_2, SiO_2, Al_2O_3, and MgO with similar Ru dispersion of 0.174−0.215 (Ru surface densities: 1.1−3.1 Ru/nm^2).

The observed effects of support on ODH turnover rates (Table 1) reflect changes in the reactivity of RuO_x surfaces caused by concurrent effects of supports on RuO_x reducibility and thus on its ability to undergo reduction in kinetically relevant steps required for oxidation turnovers. Figure 1 shows incipient reduction rates for RuO_2 domains using H_2 as a stoichiometric reductant as the sample temperature increased from 298 to 793 K. Incipient reduction rates obtained by a kinetic analysis of the low-temperature part of the first reduction peak in Figure 1 are shown for each sample in Table 1. Reduction peak temperatures increased by ~30 K (416 to 447 K) as the support changed from SnO_2 to ZrO_2, TiO_2, Al_2O_3, SiO_2, and MgO. RuO_2/SnO_2 shows two additional reduction peaks at 486 K and

at >620 K (not shown), which reflect SnO_2 reduction at temperatures above those of catalytic relevance. RuO_2 domains on MgO gave two reduction features at higher temperatures, suggestive of refractory RuO_2 domains strongly interacting with MgO. H_2 consumption stoichiometries were 1.9−2.2 H_2/Ru for all samples, indicating that all Ru^{4+} cations in RuO_2 (as detected by Raman spectroscopy) reduce completely to Ru^0 during these H_2 treatments.

Initial reduction rates were extracted by kinetic analysis of the incipient reduction region of the reduction profiles[15,16] in Figure 1. These incipient reduction processes are most relevant to those occurring in nearly stoichiometric RuO_2 during the redox cycles required for methanol oxidation turnovers, evidence for which is presented below from the observed kinetic effects of CH_3OH and O_2 on catalytic oxidation rates. RuO_2 domains supported on reducible oxides (SnO_2, ZrO_2, and TiO_2) undergo more facile reduction than those supported on more insulating and refractory oxides (Al_2O_3, SiO_2, and MgO) (Table 1). If hydrogen abstraction from methoxide intermediates by lattice O-atoms is the kinetically relevant step during HCHO synthesis on RuO_x, the rates of catalytic CH_3OH oxidation and of incipient stoichiometric reduction in H_2 should increase in parallel, as indeed was found (Figure 2). These reduction rates and the corresponding CH_3OH oxidation rates (Table 1) are much higher than for previously reported catalysts based on MoO_x and VO_x domains.[2−5,15,16,18]

Supports also influence CH_3OH reaction selectivities on RuO_x-based catalysts. Support effects on selectivities are reported at ∼20% CH_3OH conversion, but the trends observed are similar at other conversion levels. Acid functions on Al_2O_3 and SiO_2 surfaces favor DMM synthesis (57.4 and 56.1% selectivity), but MF also forms (30.1 and 31.0%). Supports, such as SnO_2, ZrO_2, and TiO_2, with amphoteric surfaces or known hydrogenation−dehydrogenation functions, preferentially formed MF (60.7−70.7%; Table 1). These effects of supports on selectivity indicate that secondary reactions of primary HCHO products can occur on support surfaces or that such surfaces can intercept reaction intermediates (i.e., CH_3OCH_2OH) required for DMM or MF syntheses.

The role of supports in catalyzing HCHO−CH_3OH reactions or in some manner directing reaction intermediates toward a given product was confirmed by physically mixing supported RuO_2 catalysts with additional amounts of various pure supports. Al_2O_3 addition to RuO_2/TiO_2 (3:1 support/catalyst mass; 393 K) increased DMM selectivities from 8.9 to 41.9%, while MF selectivity decreased from 65.2 to 45.2% (Table 2). Thus, Al_2O_3 supports, even in pure form, directed HCHO−CH_3OH reactions toward DMM, decreasing the availability of HCHO (or its intermediate reaction products) for MF synthesis on the RuO_2/TiO_2 component of this composite catalyst. Conversely, DMM selectivities on RuO_2/Al_2O_3 decreased from 57.4 to 32.6% when pure TiO_2 (3:1 mass ratio) was added, while the MF selectivity markedly increased from 30.1 to 60.4%; thus, TiO_2 surfaces either converted HCHO−CH_3OH mixtures to MF or scavenged reactive gas-phase intermediates (e.g., CH_3OCH_2OH; Scheme 1) that would have otherwise formed DMM on Al_2O_3 acid sites and directed them instead toward MF synthesis on RuO_x domains. Oxidative dehydrogenation rates were not influenced by mixing pure supports, consistent with the required involvement of RuO_x domains in the initial HCHO synthesis step. CH_3OH consumption rates changed only to the extent required to satisfy the different CH_3OH stoichiometric requirements for DMM and MF synthesis in secondary CH_3OH−HCHO reactions (Scheme 1).

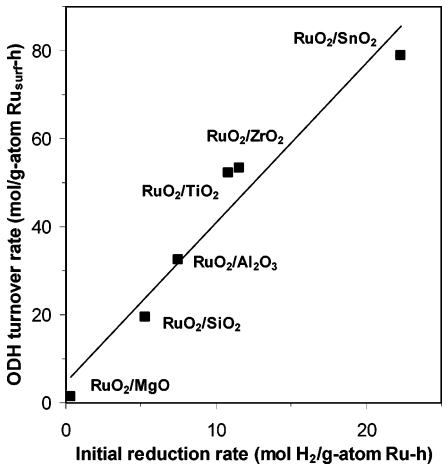

Figure 2. Dependence of rates of oxidative dehydrogenation (per g-atom surface Ru) of CH_3OH to HCHO at 393 K on initial reduction rates in H_2 (per g-atom Ru) at 403 K for RuO_2 domains supported on SnO_2, ZrO_2, TiO_2, SiO_2, Al_2O_3, and MgO with similar Ru dispersion of 0.174−0.215 (Ru surface densities: 1.1−3.1 Ru/nm^2).

A plausible sequence of elementary steps for methanol oxidation on RuO_x domains is shown as steps 1−4 below; it is consistent with the results presented above and with HCHO synthesis pathways previously proposed.[1,5,7,8]

$$CH_3OH + \text{-O*-Ru-O*-Ru-O*-} \leftrightarrow \{\text{-O*-Ru-OCH}_3\ \text{HO*-Ru-O*-}\} \quad (1)$$

$$\{\text{-O*-Ru-OCH}_3\ \text{HO*-Ru-O*-}\} \rightarrow \{\text{HO*-Ru-O*-Ru-*OH }\} + HCHO \quad (2)$$

$$\{\text{HO*-Ru-O*-Ru-*OH }\} \rightarrow H_2O^* + \{\text{-O*-Ru-O*-Ru-}\square\} \quad (3)$$

$$O_2 + \{\text{-O*-Ru-O*-Ru-}\square\} \rightarrow \{\text{-O*-Ru-O*-Ru-(O}_2\text{)}\} \rightarrow \cdots\cdots \quad (4)$$

In this sequence, the {-O*-Ru-O*-Ru-O*-} is meant to depict in general RuO_x structures with reactive lattice oxygen atoms (O*). These postulated elementary steps include dissociative CH_3OH chemisorption to form methoxide (CH_3O^-) intermediates (Step 1), followed by hydrogen abstraction from CH_3O^- using lattice oxygen atoms (O*) in RuO_x to form HCHO (Step 2). H_2O desorption via recombination of OH groups forms an oxygen vacancy (□) (Step 3), and O_2 dissociative chemisorption (Step 4) ultimately restores the missing lattice oxygen in a series of steps that complete a Mars-van Krevelen redox cycle.[1,19] These steps are consistent with the kinetic dependence of reaction rates on CH_3OH and O_2 partial pressures, as we discuss next.

Figure 3 shows CH_3OH oxidative dehydrogenation rates and product selectivities as a function of CH_3OH partial pressure (0−40 kPa) at 393 K and 9 kPa O_2 on RuO_2/TiO_2 (3.1 Ru/nm^2). At similar conversions (∼10%), ODH rates first increased almost linearly with increasing CH_3OH pressure (below 8 kPa) and then more gradually, ultimately reaching nearly constant values above 12 kPa. This behavior indicates that active surfaces become saturated with CH_3OH-derived reactive intermediates (e.g., CH_3O^-) as CH_3OH pressure increases. In parallel, MF and DMM selectivities increased (from 56.9 and 1.5%, respectively) and approached constant values (80.2 and 9.1%) with increasing CH_3OH partial pressures; HCHO selectivities concurrently decreased from 42.5 to 10.3%. CO_x selectivities were very

TABLE 2: Methanol Oxidation Rates and Selectivities on Physical Mixtures of $RuO_2/TiO_2 + Al_2O_3$, and $RuO_2/Al_2O_3 + TiO_2$ at a Mass Ratio of 1/3, and for Comparison on RuO_2/TiO_2 (6.2 Ru/nm^2) and RuO_2/Al_2O_3 (1.3 Ru/nm^2)[a]

catalyst (mass ratio)	CH_3OH conversion rate (mol/g-atom Ru-h)	calculated ODH rate[b] (mol/g-atom Ru-h)	selectivity (% carbon)			
			HCHO	MF	DMM	CO_x
$RuO_2/TiO_2 + Al_2O_3$ (1/3)	12.6	6.1	11.6	45.2	41.9	1.4
$RuO_2/Al_2O_3 + TiO_2$ (1/3)	13.8	6.5	6.2	60.4	32.6	0.8
RuO_2/TiO_2	10.9	6.6	24.9	65.2	8.9	1.0
RuO_2/Al_2O_3	14.9	6.8	11.6	30.1	57.4	1.0

[a] 393 K, 4% CH_3OH, 9% O_2, 1% N_2, ~20% CH_3OH conversion. [b] Rate for primary CH_3OH oxidative dehydrogenation to HCHO.

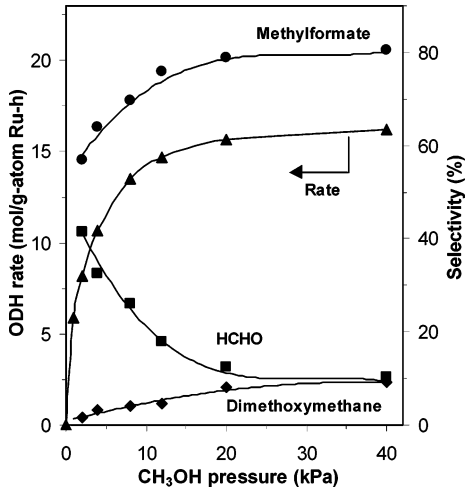

Figure 3. Effect of methanol partial pressure on rates of oxidative dehydrogenation (per g-atom Ru) of CH_3OH to HCHO and selectivities at 393 K on RuO_2/TiO_2 (3.1 Ru/nm^2, 9 kPa O_2, 1 kPa N_2, balance He, CH_3OH conversion: ~10%).

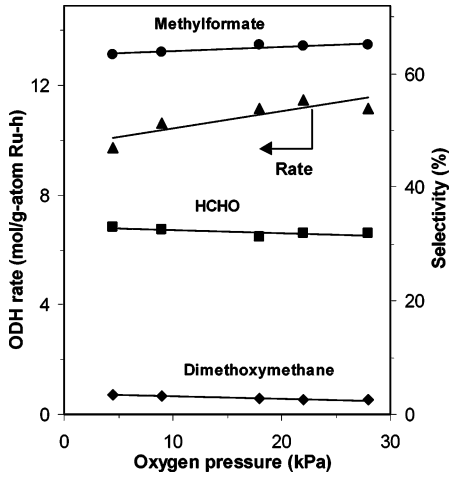

Figure 4. Effect of oxygen partial pressure on rates of oxidative dehydrogenation (per g-atom Ru) of CH_3OH to HCHO and selectivities at 393 K on RuO_2/TiO_2 (3.1 Ru/nm^2, 4 kPa CH_3OH, balance He, CH_3OH conversion: ~10%).

low (<1%), and they are not shown in Figure 3. These selectivity trends reflect the secondary nature of reaction pathways leading to MF and DMM synthesis, which require sequential bimolecular coupling between HCHO and CH_3OH-derived intermediates (Scheme 1), the rate of which depends on pressure more sensitively than initial HCHO synthesis rates.

Figure 4 shows the effects of O_2 partial pressure on oxidative CH_3OH dehydrogenation rates and product selectivities on RuO_2/TiO_2 (3.1 Ru/nm^2) (393 K, 4 kPa CH_3OH). Reaction rates and selectivities were essentially unaffected by O_2 partial pressures (4.5−28 kPa). Such kinetic insensitivity to O_2 concentrations is typical of catalytic oxidation reactions proceeding via Mars-van Krevelen mechanism[19] using lattice oxygen atoms on nearly stoichiometric surfaces, a finding confirmed by anaerobic transient CH_3OH reaction data reported below. Measurements at 20 kPa CH_3OH and varying O_2 concentrations led to essentially identical trends and conclusions.

TABLE 3: Kinetic Isotopic Effects for Methanol Oxidation on RuO_2/TiO_2 at 393 K[a]

	CH_3OH conversion rate (mol/g-atom Ru-h)	calculated ODH rate[b] (mol/g-atom Ru-h)	MF synthesis rate (mol/g-atom Ru-h)
CH_3OH	16.3	10.5	11.4
CH_3OD	15.8	10.3	10.9
CD_3OD	6.5	4.4	3.7
k_{CH_3OH}/k_{CH_3OD}	1.03	1.02 (1.11)[c]	1.05
k_{CH_3OH}/k_{CD_3OD}	2.51	2.38 (3.33)[c]	3.07

[a] 3.1 Ru/nm^2, 4% methanol, 9% O_2, ~10% methanol conversion. [b] Rate for primary methanol oxidative dehydrogenation to formaldehyde. [c] Data in parentheses were obtained on $Fe_2(MoO_4)_3$ at 473 K from ref 20.

Methanol molecules deuterated at all positions (CD_3OD) or only at the hydroxyl group (CH_3OD) were used to probe the kinetic relevance of elementary steps involving methoxide formation and H-abstraction from methoxide during CH_3OH oxidation on RuO_x domains. Kinetically relevant methanol dissociation steps would lead to normal kinetic isotope effects (KIE) for both CH_3OD and CD_3OD reactants. In contrast, the kinetic relevance of H-abstraction from CH_3O^- to form HCHO would lead to normal KIE for CD_3OD and weak thermodynamic isotope effects for CH_3OD.

Table 3 shows kinetic isotope effects (defined as the ratio of ODH rates for undeuterated and deuterated methanol) measured at 4 kPa methanol and 9 kPa O_2 on RuO_2/TiO_2 at 393 K. At these conditions, oxidation rates are linear in methanol concentration and independent of O_2 pressure (Figures 3 and 4). CD_3OD reactants gave kinetic isotope effects greater than 2 for the rate of each reaction (methanol total conversion, oxidative dehydrogenation, and methylformate synthesis). In contrast, each of these rates was almost unchanged when CH_3OD was used instead of CH_3OH as reactants (KIE values of 1.02−1.05). Thus, deuterium substitution at the methanol hydroxyl group is kinetically inconsequential, indicating that dissociative chemisorption to form methoxide species is quasi-equilibrated during oxidative CH_3OH dehydrogenation on RuO_x domains.

These CD_3OD and CH_3OD kinetic isotope effects resemble those measured for HCHO synthesis on $Fe_2(MoO_4)_3$ at 473 K (Table 3),[20] which led to conclusions about the kinetic relevance of methoxide C−H bond activation similar to those reached here for RuO_x-based catalysts. CD_3OD KIE values on RuO_x domains are smaller than on $Fe_2(MoO_4)_3$, even though the lower temperatures used on RuO_x catalysts would typically lead to larger isotope effects for identical reaction coordinate and rate-determining step. This appears to indicate that transition states retain more reactant character during H-abstraction on RuO_x

catalysts; C−D and C−H bonds are consequently less disrupted within the activated complex along the reaction coordinate on RuO_x than on $Fe_2(MoO_4)_3$ catalysts. This leads, in turn, to smaller differences in reactivity between molecules containing C−H and C−D bonds. This shift toward reactant-like activated complexes becomes stronger as elementary steps become more exothermic, a process that also leads to lower activation energies, through ubiquitous Bronsted-Polanyi-type relations between kinetic and thermodynamic parameters, and to higher reaction rates. Thus, the lower KIE values measured on RuO_x catalysts are consistent with the observed ability of these materials to catalyze the overall reaction sequence, and the kinetically relevant H-abstraction step, more effectively (and at lower temperatures) than $Fe_2(MoO_4)_3$.

The involvement of lattice oxygen atoms in CH_3OH oxidation was confirmed by transient CH_3OH reactions without O_2 co-reactants on RuO_2/TiO_2 at 393 K. These data were obtained by removing reactants and reactive intermediates using a pure He purge for 300 s after steady-state catalytic reactions of CH_3OH-O_2 mixtures were carried out for 1.5 h, and then introducing a CH_3OH-containing stream without O_2 co-reactants. Figure 5a,b show that removal of O_2 from the reactant mixture did not initially influence ODH (or MF synthesis) rates or selectivities, indicating that lattice oxygen atoms are sufficient to form all reaction products observed during steady-state oxidation catalysis. These anaerobic rates decreased with time as lattice oxygen was gradually depleted by CH_3OH oxidation events. In the process, methanol conversion decreased, leading to changes in product selectivity consistent with those obtained when conversion was varied instead by changing residence time (Figure 5b). The reintroduction of O_2 into the CH_3OH stream led to the rapid and complete recovery of the initial catalytic CH_3OH conversion rates and selectivities (Figure 5a).

The characteristic time for reoxidation during these transients was much shorter than for oxygen depletion, consistent with rapid and kinetically irrelevant reoxidation steps and with low steady-state concentrations of oxygen vacancies during catalysis, as suggested by the kinetic analysis and mechanistic proposals described. The initial decay in methanol conversion rates with time can be accurately described by a first-order dependence on the concentration of remaining lattice oxygen atoms. The time constant obtained from fitting the resulting exponential function in time led to a turnover rate estimate of 33 h^{-1}, which resembles steady-state turnover rates measured before and after these anaerobic transients and based on the dispersion of RuO_2 clusters after reduction in H_2 (53 h^{-1}). This agreement, although qualitative, is nevertheless remarkable; it confirms the accuracy of dispersion measurements and suggests that all lattice oxygen atoms in RuO_2 domains exhibit similar reactivity in H-abstraction reactions.

This transient behavior is characteristic of catalytic oxidations proceeding via Mars-van Krevelen mechanisms using lattice oxygen atoms. About 1.2 oxygen atoms were removed per Ru from RuO_2 domains dispersed on TiO_2 before methanol oxidation catalysis was suppressed; similar oxygen removal stoichiometries (O/Ru = 1.1−1.3) were observed for RuO_x domains supported on ZrO_2 and Al_2O_3. These values indicate that RuO_2 species prevalent during steady-state catalysis become unreactive as lattice oxygen is removed and the system undergoes a two-electron reduction of Ru^{4+} centers ($Ru^{4+} \rightarrow Ru^{2+}$) during anaerobic CH_3OH reactions; they also show that reduction to Ru^0 does not occur during either aerobic or anaerobic oxidation of CH_3OH at conditions required for these reactions and that RuO species are unreactive in methanol activation at these

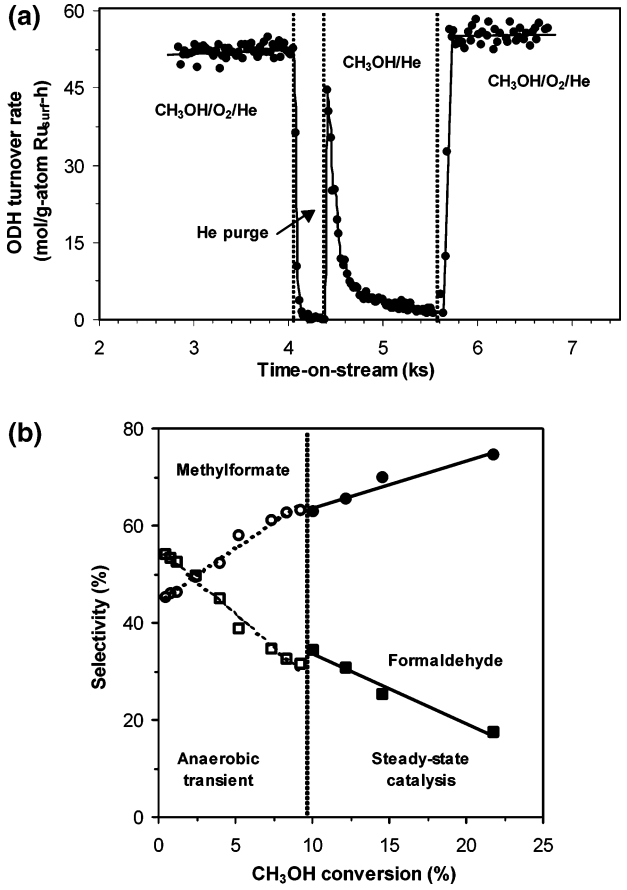

Figure 5. Oxidative dehydrogenation turnover rates (a) and HCHO and MF selectivities (b) during steady-state catalysis and during transient anaerobic oxidation of CH_3OH on RuO_2/TiO_2. Conversion was varied by changing space velocity during steady-state catalysis and by allowing lattice oxygen depletion during anaerobic transients (3.1 Ru/nm^2, 4 kPa CH_3OH, 9 kPa O_2 or no O_2, balance He).

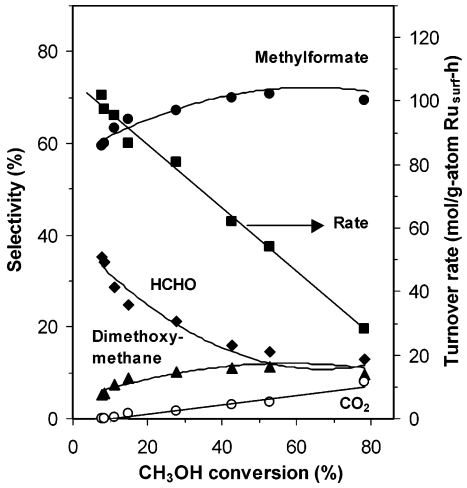

Figure 6. CH_3OH conversion turnover rates and selectivities as a function of CH_3OH conversion changed by varying residence time (18−610 g-atom Ru-s/mol CH_3OH) at 393 K on RuO_2/TiO_2 (6.2 Ru/nm^2, fractional Ru dispersion: 0.125, 4 kPa CH_3OH, 9 kPa O_2, 1 kPa N_2, balance He).

reaction conditions. These conclusions are consistent with the weak kinetic consequences of O_2 concentration on catalytic CH_3OH oxidation rates (Figure 4).

Figure 6 shows the effects of CH_3OH conversion, changed by varying residence time, on CH_3OH conversion turnover rates and product selectivities at 393 K on RuO_2/TiO_2 (6.2 Ru/nm^2).

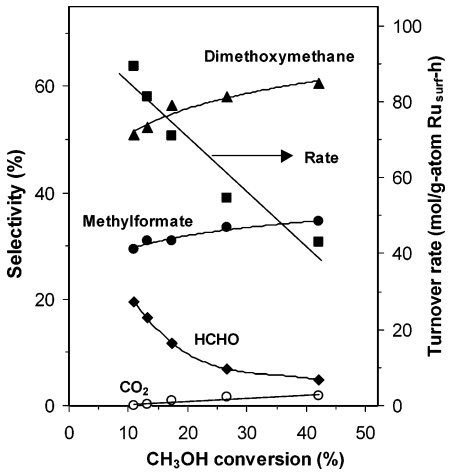

Figure 7. CH_3OH conversion turnover rates and selectivities as a function of CH_3OH conversion changed by varying residence time (35−290 g-atom Ru-s/mol CH_3OH) at 393 K on RuO_2/Al_2O_3 (1.3 Ru/nm^2, fractional Ru dispersion: 0.209, 4 kPa CH_3OH, 9 kPa O_2, 1 kPa N_2, balance He).

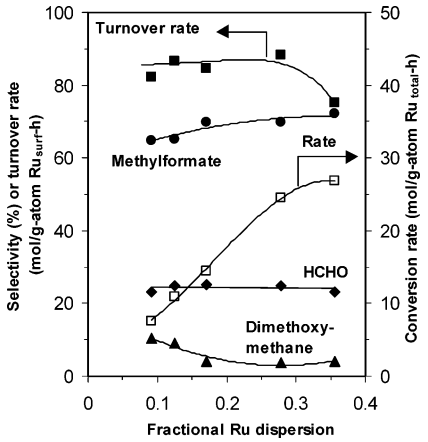

Figure 8. CH_3OH oxidation rates and selectivities as a function of fractional Ru dispersion at 393 K on RuO_2/TiO_2 at conversions of ∼15−20% (0.8−13.1 Ru/nm^2, 4 kPa CH_3OH, 9 kPa O_2, 1 kPa N_2, balance He).

Turnover rates decreased with increasing residence time (and CH_3OH conversion) as a result of reactant depletion, combined with weak kinetic inhibition effects by water co-products formed in oxidative dehydrogenation and condensation reactions. MF and DMM selectivities increased with increasing CH_3OH conversion, while HCHO selectivity concurrently decreased, as expected from sequential pathways involving HCHO intermediates and the formation of MF and DMM. The nonzero MF selectivities observed as conversion decreases indicate that MF can be formed to some extent directly from CH_3OH, but also via readsorption of desorbed HCHO initial products, which tends to be favored as the concentration of HCHO increases with increasing residence time. CO_2 selectivities were low (0−8%) and increased with increasing residence time, suggesting that CO_2 forms predominately via sequential oxidation or decomposition of HCHO, MF, and DMM products, and not via direct combustion of CH_3OH reactants. No CO was detected at any reaction conditions, as expected from the high CO oxidation rates reported on RuO_x surfaces.[11] Similar residence time effects on CH_3OH conversion turnover rates and selectivities were observed on RuO_2/Al_2O_3 (1.3 Ru/nm^2), on which DMM instead of MF is preferentially formed (Figure 7). This indicates that CH_3OH oxidative conversion proceeds via similar reaction pathways (Scheme 1) on RuO_x domains dispersed on both supports.

These residence time and support effects suggest that CH_3OH initially forms HCHO, which then reacts to form DMM and MF via methoxymethanol (CH_3OCH_2OH) intermediates or hemiacetal adsorbed species.[7] HCHO acetalization with nucleophilic methoxides (CH_3O) can lead to CH_3OCH_2OH intermediates,[5,21−23] which condense with CH_3OH on acid sites to form DMM in equilibrium-constrained reactions, or dehydrogenate on redox sites to form MF (and H_2O) in thermodynamically favored reactions catalyzed by either RuO_x domains or active supports. These reactions occur, at least in part, on support surfaces containing acid or dehydrogenation sites, leading to the observed effects of supports on selectivity. Molecular simulations have suggested that CH_3OCH_2OH dehydrogenation forms MF much faster than HCHO dimerization (Tischenko reaction) or CH_3OH reactions with adsorbed formate ($HCOO^-$) on V_2O_5.[22] CH_3OCH_2OH was not detected during our study of CH_3OH reactions on RuO_x, apparently because of its unfavorable equilibrium and high reactivity.

CH_3OH reaction rates (per Ru-atom) increased almost linearly with increasing Ru dispersion (changed by varying Ru content from 0.6 to 8.2 wt %) on TiO_2, indicating that turnover rates are essentially insensitive to RuO_2 domain size in this dispersion range (Figure 8). The slightly lower turnover rate measured on the sample with the highest Ru dispersion reflects the lower reducibility expected for the prevalent small oxide domains,[15] which was confirmed by H_2 reduction rate measurements. Selectivities were influenced weakly by Ru content and dispersion. MF selectivities (at 15−20% CH_3OH conversion) increased slightly as dispersion increased (Figure 8), a trend that merely reflects a concomitant increase in exposed TiO_2 surfaces, which catalyze secondary reactions of HCHO to form MF, relative to exposed RuO_x surfaces, which are required to form the required HCHO intermediates.

These RuO_x catalysts are compared with previously reported CH_3OH oxidation catalysts in Table 1. $V_2O_5-TiO_2$ prepared by coprecipitation and MoO_3/SiO_2 prepared via impregnation method catalyze MF synthesis with high selectivity (∼80 and 95.9%, at ∼75 and 5% conversion, respectively);[2,5] reaction rates are much lower than on RuO_x catalysts, even at the higher temperatures of these previous studies. RuO_2/TiO_2 (4.1 wt %), gave reaction rates of 4.8 mol/g-atom Ru_{total}-h at 78.2% CH_3OH conversion and 393 K (Figure 6), which exceed those reported on $V_2O_5-TiO_2$ (∼3.4 mol/g-atom V_{total}-h at ∼80% CH_3OH conversion) at 433 K, with comparable MF and CO_2 selectivities of 70.4 and 7.9% (vs 80 and 5%), respectively. High MF selectivities (∼90%) have also been reported on Mo−Sn mixed oxides at 433 K at low reaction rates,[3] but similar compositions led to much lower MF selectivities (47% at ∼40% CH_3OH) at 453 K in another study.[4]

RuO_2/SiO_2 (1.1 Ru/nm^2) and RuO_2/SnO_2 (2.5 Ru/nm^2) also convert ethanol-O_2 reactant mixtures with high rates and selectivity to form acetaldehyde, diethoxyethane (acetal), and ethyl acetate at 393 K (Table 4). Neither diethyl ether nor CO_x products were detected. As in methanol reactions, ethanol oxidation turnover rates were higher when RuO_2 domains were supported on SnO_2 than on SiO_2. Ethanol conversion rates increased with pressure and then reached a constant value; as C_2H_5OH pressure increased from 2 to 40 kPa, products shifted from acetaldehyde (97.3 to 17.6%), formed in primary oxidative dehydrogenation steps, to diethoxyethane (0 to 81%), which forms via condensation reactions favored kinetically and thermodynamically at higher C_2H_5OH pressures (Table 4). Residence time effects on selectivities showed that reaction

TABLE 4: Ethanol Oxidation Rates and Selectivities on RuO_2/SiO_2 (1.1 Ru/nm^2) and RuO_2/SnO_2 (2.5 Ru/nm^2) at 393 K[a]

catalyst	C_2H_5OH pressure (kPa)	ethanol conversion turnover rate (mol/g-atom Ru_{surf}-h)	ODH turnover rate[b] (mol/g-atom Ru_{total}-h)	selectivity (%)			
				acetaldehyde	ethyl acetate	acetal	CO_x
RuO_2/SiO_2	4	30.6	30.1	97.1	0	2.9	0
RuO_2/SnO_2	2	51.6	50.9	97.3	2.7	0	0
RuO_2/SnO_2	4	76.3	73.2	93.4	2.0	4.6	0
RuO_2/SnO_2	10	108.6	83.5	64.8	2.2	33.0	0
RuO_2/SnO_2	20	157.4	86.1	30.8	1.2	68.0	0
RuO_2/SnO_2	40	188.9	85.9	17.6	1.4	81.0	0

[a] 9 kPa O_2, 1 kPa N_2, ~10−15% C_2H_5OH conversion. [b] Rate for primary oxidative dehydrogenation of C_2H_5OH to acetaldehyde.

pathways involve initial acetaldehyde formation in oxidative dehydrogenation steps and subsequent acetalization reactions of acetaldehyde and ethanol to form diethoxyethane.

To our knowledge, these supported RuO_x materials have not been previously used for the activation and conversion of CH_3OH, C_2H_5OH, or other short-chain alcohols, even though Ru oxides catalyze the oxidation of more reactive C_{5+} alcohols in the liquid phase to form aldehydes and ketones at ~373 K.[12−14] Idriss and co-workers[24] adsorbed methanol on RuO_2 and only ~0.6% of the adsorbed methanol formed methylformate in stoichiometric reactions of methanol preadsorbed at ambient temperature. In this study, the reduction of RuO_2 to Ru metal at 573 K in H_2 led to higher stoichiometric MF yields (~11%), via non-oxidative reactions unrelated to those prevalent on RuO_2.[24] These previous studies did not detect or report evidence for the remarkable activity and selectivity shown here for RuO_x-based materials in selective oxidation reactions of CH_3OH and C_2H_5OH.

In marked contrast, the supported RuO_2 domains reported here gave unprecedented CH_3OH conversion rates and allow CH_3OH oxidation reactions to proceed at significant rates near ambient temperatures with >99% combined selectivities to useful formaldehyde, methylformate, and dimethoxymethane products. The mechanistic details and the marked effects of support on rate and selectivity reported here suggest significant opportunities for the kinetic coupling of these low-temperature oxidative CH_3OH activation pathways with other catalytic functions, such as condensation, methylation, and hydration reactions of HCHO, MF, and DMM to form more complex oxygenate molecules, including those containing new C−C bonds. The unique behavior of these supported RuO_2 clusters is not restricted to CH_3OH activation reactions, and it appears to extend to higher alcohols,[25] thus providing opportunities for also converting ethanol to diethoxyethane (acetal) and acetaldehyde with high rates and selectivities near ambient temperatures.

4. Conclusions

Supported RuO_2 domains on SnO_2, ZrO_2, TiO_2, Al_2O_3, and SiO_2 provide low-temperature paths for CH_3OH activation to form HCHO and for its subsequent conversion to MF and DMM. The unprecedented ability of these materials to catalyze oxidative CH_3OH near ambient temperatures leads to favorable thermodynamics and to selective kinetic paths for the formation of the products. This unique reactivity reflects the ability of small RuO_2 domains to undergo fast redox cycles without significant formation of unselective Ru metal clusters. Turnover rates and selectivities depend on the nature of the support, which influences RuO_2 reducibility and thus the rate of kinetically relevant hydrogen abstraction from adsorbed methoxide intermediates. The kinetic effects of CH_3OH and O_2 reactant concentrations and the results of transient anaerobic measurements are consistent with Mars-van Krevelen redox mechanisms requiring lattice oxygen atoms. CD_3OD reactants led to normal kinetic isotope effects, while CH_3OD and CH_3OH oxidation rates were nearly identical, consistent with quasi-equilibrated methoxide formation and rate-determining H-abstraction from methoxide intermediates. DMM forms via acid-catalyzed secondary reactions of CH_3OH with intermediates derived from CH_3OH−HCHO acetalization reactions on support acid sites, while MF appears to form via H-abstraction from these intermediates on RuO_2 or support redox active sites. Acid sites on Al_2O_3 and SiO_2 favor dimethoxymethane formation, while redox and amphoteric sites on SnO_2, ZrO_2, and TiO_2 preferentially form methylformate. The effects of residence time and of mixing pure supports with supported RuO_2 catalysts are consistent with these conclusions. These materials also catalyze the selective oxidation of ethanol to acetaldehyde and diethoxyethane at 300−400 K.

Acknowledgment. The authors dedicate this manuscript to Professor Michel Boudart on the occasion of his 80th birthday and acknowledge with thanks his pioneering contributions to the science and applications of catalysis, as well as his mentorship of several generations of students, colleagues, and friends. This work was supported by BP as part of the Methane Conversion Cooperative Research Program at the University of California at Berkeley. This work was also supported in part by the Director, Office of Basic Energy Sciences, Chemical Sciences Division of the U.S. Department of Energy under Contract DE-AC03-76SF00098. The authors acknowledge the assistance of Ms. Patricia Cheung with the anaerobic transient experiments, as well as helpful technical discussions with Dr. Theo Fleisch of BP during the early stages of this study.

References and Notes

(1) Tatibouet, J. M. *Appl. Catal. A* **1997**, *148*, 213.
(2) Tronconi, E.; Elmi, A. S.; Ferlazzo, N.; Forzatti, P.; Busca, G.; Tittarelli, P. *Ind. Eng. Chem. Res.* **1987**, *26*, 1269.
(3) Ai, M. *J. Catal*. **1982**, *77*, 279.
(4) Valente, N. G.; Arrua, L. A.; Cadus, L. E. *Appl. Catal. A* **2001**, *205*, 201.
(5) Louis, C.; Tatibout, J. M.; Che, M. *J. Catal*. **1988**, *109*, 354.
(6) Yuan, Y.; Iwasawa, Y. *J. Phys. Chem. B* **2002**, *106*, 4441.
(7) Liu, H.; Iglesia, E. *J. Phys. Chem. B* **2003**, *107*, 10840.
(8) Busca, G. *Catal. Today* **1996**, *27*, 457.
(9) Liu, Y. C.; Griffin, G. L.; Chan, S. S.; Wachs, I. E. *J. Catal*. **1985**, *94*, 108.
(10) Kolah, A. K.; Mahajani, S. M.; Sharma, M. M. *Ind. Eng. Chem. Res*. **1996**, *35*, 3707.
(11) Zang, L.; Kisch, H. *Angew. Chem., Int. Ed.* **2000**, *39*, 3921.
(12) Zhan, B. Z.; White, M. A.; Sham, T. K.; Pincock, J. A.; Doucet, R. J.; Rao, K. V. R.; Robertson, K. N.; Cameron, T. S. *J. Am. Chem. Soc.* **2003**, *125*, 2195.
(13) Yamaguchi, K.; Mizuno, N. *Angew. Chem., Int. Ed*. **2002**, *41*, 4538.
(14) Musawir, M.; Davey, P. N.; Kelly, G.; Kozhevnikov, I. V. *J. Chem. Soc. Chem. Commun.* **2003**, 1414.
(15) Liu, H.; Cheung, P.; Iglesia, E. *J. Catal*. **2003**, *217*, 222.

(16) Chen, K.; Xie, S.; Bell, A. T.; Iglesia, E. *J. Catal*. **2001**, *198*, 232.
(17) Mar, S. Y.; Chen, C. S.; Huang, Y. S.; Tiong, K. K. *Appl. Surf. Sci*. **1995**, *90*, 497.
(18) Desikan, A. N.; Zhang, W.; Oyama, S. T. *J. Catal*. **1995**, *157*, 740.
(19) Mars, P.; van Krevelen, D. W. *Chem. Eng. Sci*. **1954**, *3*, 41.
(20) Machiels, C. J.; Sleight, A. W. *J. Catal*. **1982**, *76*, 238.
(21) Wachs, I. E.; Madix, R. J. *Surf. Sci*. **1978**, *76*, 531.
(22) Sabeth, J.; Juan, A.; Gambaro, L.; Thomas, H. *J. Mol. Catal. A* **1997**, *118*, 283.
(23) Tatibouet, J. M.; Lauron-Pernot, H. *J. Mol. Catal. A* **2001**, *171*, 205.
(24) Madhavaram, H.; Idriss, H.; Wendt, S.; Kim, Y. D.; Knapp, M.; Over, H.; Assmann, J.; Loffler, E.; Muhler, M. *J. Catal*. **2001**, *202*, 296.
(25) Liu, H.; Iglesia, E. U.S. Patent Application, 2003.